The Korean Journal of Ceramics, **3** [2] 73 - 81 (1997)

Estimation of Interfacial Adhesion through the Micromechanical Analysis of Failure Mechanisms in DLC Film

Jeung-Hyun Jeong, Hae-Seok Park, Jeong-Hoon Ahn and Dongil Kwon

Division of Materials Science and Engineering, Seoul National University, Seoul 151-742, Korea
(Received November 5, 1996)

In this paper, it is intended to present more reproducible and quantitative method for adhesion assessment. In scratch test, micromechanical analysis on the stress state beneath the indenter was carried out considering the additional blister field The interface adhesion was quantified as work of adhesion through Griffith energy approach on the basis of the analyzed stress state. The work of adhesion for DLC film/WC-Co substrate calculated through the proposed analysis shows the identical value regardless of distinctly different critical loads measured with the change of film thickness and scratching speed. On the other hand, uniaxial loading was imposed on DLC film/Al substrate, developing the transverse film cracks perpendicular to loading direction. Since this film cracking behavior depends on the relative magnitude of adhesion strength to film fracture strength, the quantification of adhesion strength was given a trial through the micromechanical analysis of adhesion-dependence of film cracking patterns. The interface shear strength can be quantified from the measurement of strain ε_s and crack spacing λ_s at the cessation of film cracking.

Key words : Scratch test, Blister stress, Work of adhesion, Film cracks, Interface shear strength

I. Introduction

Since hard films such as diamond, diamond-like carbon (DLC) and TiN have excellent properties of hardness, wear resistance, lubrication, etc., they have been widely used as optical coatings, protective coatings, and so on. However, their service quality is significantly influenced by adhesion loss resulting from mechanical or thermal stress, humidity, etc., during fabrication or service. To ensure the mechanical reliability of films, therefore, systematic studies on the quantitative and repeatable adhesion test must be performed. Accordingly, to assess adhesion performance, many techniques have been developed and used, such as peel test, pull-off test, etc. However, these tests are limited by adhesive strength and lack of repeatability. In addition, in the widely used scratch test, test results are strongly affected by several parameters related to the testing conditions and to the coating/substrate system, and it is not easy to deduce absolute values of adhesion since the process of scratch formation is very complex. Hence, we analyze the stress state ahead of the indenter and then evaluate the interface adhesion strength. Moreover, the so-called film cracking technique has been introduced especially for a hard film/soft substrate system, as a comparative and complementary technique for the other tests and several analyses of current test have been presented.[1-5]

II. Modeling

1. Scratch test

In scratch tests, delamination at the interface between the brittle film and the substrate occurs in the region ahead of the indenter, where the compressive stress develops. The test has been analyzed in terms of three contributions to the delamination between film and substrate: (1) a static indentation stress; (2) a friction stress due to the interactions between the sliding indenter and the specimen surface; (3) a residual stress in the film.

When a specimen is indented by a hard sphere, a symmetric stress distribution develops in which the three principal stresses are compressive, on the surface and beneath the contact region and to a depth of the order of the contact diameter. Outside the contact region there exist a radial tensile stress and a hoop stress, each of which takes on its maximum value at the edge of the contact region.[6] The surface stress and strain fields are independent of the contact stress distribution generated by the indenting load, assuming the same total indenting load L and a radially symmetric stress distribution inside the contact region.[7-9] When plastic deformation of the substrate occurs beneath the indenter, the stress analysis based on the elastic deformation is inappropriate. The appropriate elastic stress field for an elastic-plastic indentation can be obtained by considering the blister stress generated by the plastically deformed substrate;[10,11] this blister stress is proportional to $1/r^3$, where r is the distance from the center of the indenter.

In addition, the friction effect generated by the interaction between the sliding indenter and the surface of the specimen must be considered. This friction stress

field generated by a sliding indenter can be derived by regarding the indenting load as a symmetric stress distribution within the contact region.[7] This friction effect leads to stress enhancement over the indentation stress field and also induces a compressive stress at the leading edge, resulting in the strong compression of the film in front of the indenter. Thus the total elastic stress field acting at the leading edge is

$$\sigma_{xx} = -\frac{L}{2\pi a^2}\left[(1-2\nu_s)-(4+\nu_s)\frac{3\pi\mu}{8}\right]-\frac{B}{a^3}4(2-\nu_s)$$
$$\sigma_{yy} = -\frac{L}{2\pi a^2}\left[(1-2\nu_s)+\frac{9\pi\nu_s\mu}{8}\right]+\frac{B}{a^3}4(1-2\nu_s) \quad (1)$$
$$\sigma_{zz} = \sigma_{xy} = \sigma_{yz} = \sigma_{zx} = 0$$

where L is the indenting load, a is the contact radius, ν_s is the Poisson's ratio of substrate, μ is the friction coefficient between the indenter and the film, and B is a constant.

From this stress analysis,[12] we can derive the strain field of the film ahead of the indenter. The strain fields of the film and the substrate are expected to be the same at the interface under the condition that the adherence between film and substrate must be maintained at the interface, and the film is thin enough that the strain in film may not decrease significantly over the film thickness. Then the film strain field can be expressed as

$$\varepsilon_{xx} = \frac{1}{E_s}\left[\frac{L}{2\pi a^2}(1+\nu_s)\left[(1-2\nu_s)-(4-3\nu_s)\frac{3\pi\mu}{8}\right]\right.$$
$$\left.-\frac{B}{a^3}8(1-\nu_s)(1+\nu_s)\right] \quad (2)$$
$$\varepsilon_{yy} = \frac{1}{E_s}\left[-\frac{L}{2\pi a^2}(1+\nu_s)\left[(1-2\nu_s)-\frac{3\pi\nu_s\mu}{8}\right]\right.$$
$$\left.+\frac{B}{a^3}4(1-\nu_s)(1+\nu_s)\right]$$

where E_s is the Young's modulus of substrate. There also exists a small strain in the z direction, but since it cannot stretch the film, we can neglect its contribution in evaluating the elastic deformation energy stored in the film.

We can evaluate the elastic deformation energy stored in a unit volume of film using the strain field in Eq. (2). However, we must take the film residual stress into consideration. This residual stress effect can be evaluated by superposition of the residual strain on Eq. (2). Thus the elastic deformation energy can be given as

$$U_{elastic} = \frac{E_f}{2}\sum\varepsilon^2 = \frac{E_f}{2}\left[\varepsilon_{xx}^{tot^2}+\varepsilon_{yy}^{tot^2}\right]$$
$$\varepsilon_{xx}^{tot} = \frac{1}{E_s}\left[\sigma_{xx}-\nu_s\sigma_{yy}\right]+\frac{\sigma_{res}^f(1-\nu_f)}{E_f} \quad (3)$$
$$\varepsilon_{yy}^{tot} = \frac{1}{E_s}\left[\sigma_{yy}-\nu_s\sigma_{xx}\right]+\frac{\sigma_{res}^f(1-\nu_f)}{E_f}$$

where ν_f and E_f are the Poisson's ratio and the Young's modulus of the film, respectively, and σ_{res}^f is the residual stress in film.

The adhesion behavior can be modeled in terms of the strain energy which is released during film failure. At the critical load, the film ahead of the indenter reduces its elastic deformation energy by delamination and spallation of the film from the substrate. The released energy provides the surface energy for the detachment of film. Let us consider a film failure region at the critical load as a semicircular area of film of radius c detached from the substrate. The total stored energy in film is expressed as

$$U = \frac{E_f}{2}\left(\sum\varepsilon^2\right)\frac{\pi c^2 t}{2}-W\frac{\pi c^2}{2}-2(\pi+2)c\gamma_f t$$
$$W = \gamma_s+\gamma_f-\gamma_{sf} \quad (4)$$

where t is the film thickness, γ_s and γ_f are the surface energies of substrate and film, respectively, and γ_{sf} is the interfacial energy between film and substrate. On the right-hand side of Eq. (4), the first term is the elastic deformation energy stored in the film, the second is the surface and interfacial energies created by film delamination, and the last is the surface energy generated by film spallation.

The work of adhesion W represented as the interface adhesion strength is expressed by the surface and interfacial energies. If the energy released during film failure is greater than the increase of the interfacial and surface energies due to the delamination and spallation, the detachment of film will be continuous. The above condition can be expressed through the Griffith energy-balance approach:

$$W = \frac{E_f}{2}\left(\sum\varepsilon^2\right)t-\frac{2(\pi+2)}{\pi}\frac{\gamma_f}{c}t\ . \quad (5)$$

In Eq. (5), the value of γ_f/c can be estimated by assessing the elastic deformation energy stored in a unit volume of film with the change of film thickness under the same interface adhesion strength:

$$\frac{E_f}{2}\sum\varepsilon^2 = \frac{W}{t}+\frac{2(\pi+2)}{\pi}\frac{\gamma_f}{c}\ . \quad (6)$$

In other words, through plotting the elastic deformation energy stored per unit volume of film as a function of 1/t, we can obtain the value of γ_f/c as the y intercept, and the work of adhesion can be evaluated from Eq. (5) using the value of γ_f/c.

2. *Film cracking test*

Uniaxial loading of a hard-film-coated ductile substrate induces a deformation mismatch due to the different mechanical responses of film and substrate. Since strain continuity, however, must be satisfied at the interface, an interface shear stress that suppresses substrate deformation is generated. At the same time, a tensile stress σ_x^f is induced in the film, and transferred to

the film by an interface shear stress τ_i with the relation of

$$t \cdot \frac{d\sigma_x^f}{dx} = -\tau_i(x) \tag{7}$$

where x is the loading direction coordinate.

If the tensile stress transferred through relation (7) reaches the film fracture strength (σ_c), film cracking occurs.[13-15] With further loading, the number of film cracks increases first sharply and then more slowly, until finally no more cracking occurs. This asymptotic film crack spacing (Fig. 1) is related to the fact that the film tensile stress cannot reach the film fracture strength σ_c because of the failure in stress transfer by the interface damage. Because this interface damage (film separation), which occurs when the shear stress exceeds the critical shear strength τ_d, implies mode-II shear breakage of the interface, the interface shear strength can be thought as equivalent to the interface bonding force (adhesion).

The shear lag theory for fibre composites[16] was applied to the two-dimensional model of film/substrate system to analyze the stress state developed near the interface during uniaxial straining. The deformation of the ductile substrate is suppressed at the interface by the constraint of the hard film. At location more distant from the interface within the substrate, deformation is less and less suppressed, and is finally restored completely to the unconstrained deformation when the film constraint effect disappears.

The following assumptions are made in analyzing the stress state in the near-interface region: (a) The x-directional tensile stress in the film is constant over the film thickness because the film is very thin. (b) The interface shear stress has a maximum value at the interface and decreases to zero at a depth $z=\xi$ at which the film constraint effect fades away completely. ξ is defined as the distance from the interface at which the stress state of the substrate is influenced by the film constraint. (c) The interface shearing is assumed elastic because the interface shear stress is relaxed by the continuing film cracking. (d) In the near-interface region of the substrate, the external load applied to $z \leq \xi$, $\sigma_o\xi$, is assumed to be distributed into film and substrate as given in relation (8), where the x-directional tensile stress in the near-interface region of the substrate is approximated by its average $\bar{\sigma}_x^s$:

$$\sigma_o\xi = \bar{\sigma}_x^s \xi + \sigma_x^f t \tag{8}$$

where superscripts s and f represent the substrate and the film, respectively.

Through the modified shear lag analysis under these assumptions,[17] the interface shear stress can be related to the substrate displacements as follows:

$$\tau_i(x) = \frac{2G_s}{\xi}(u_s^- - u_s^i) \tag{9}$$

where u_s^- is the unconstrained displacement at $z=\xi$ and u_s^- is the film-constrained displacement at the interface (see Fig. 2). G_s is the shear modulus of substrate.

Next, combining the relation (7) and the derivative of Eq. (9) gives

$$\frac{d^2\sigma_x^f}{dx^2} = \frac{2G_s}{\xi t}\left(\frac{du_s^-}{dx} - \frac{du_s^-}{dx}\right) \tag{10}$$

where the first term on the right-hand side reflects the strain of substrate at the interface and the last term represents the strain at the film-unaffected region whose magnitude corresponds to the external strain ε.

In determining the strain components in Eq. (10), we consider separately the film residual stress effect and the film constraint effect during uniaxial straining, as depicted in Fig. 2. As seen on the right side in the figure, the film strain ε_x^f, which is constant through film thickness, is identical to the interface strain ε^i ($\varepsilon_x^f = \varepsilon^i$), when considering the film constraint effect only. The y-directional component of film stresses, which is generated in order to maintain strain continuity, is taken into account by assuming that the y component of film strain ε_y^f is nearly equal to Poisson contraction of substrate $-\nu_s\varepsilon$[18] ($\varepsilon_y^f = \varepsilon_y^s \approx -\nu_s\varepsilon$). On the other hand, the residual stress exists in the film even in the absence of stress from external

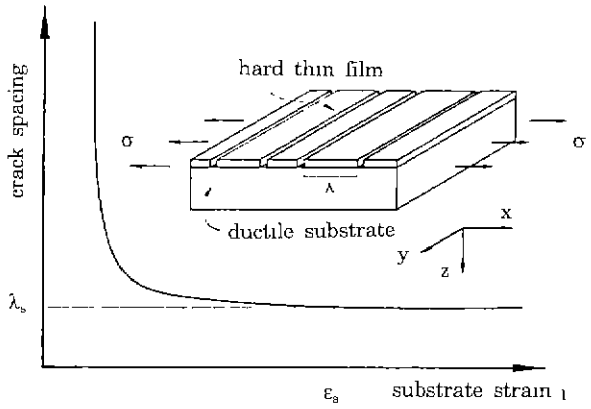

Fig. 1. Variation of film crack spacing (λ) with external strain (ε).

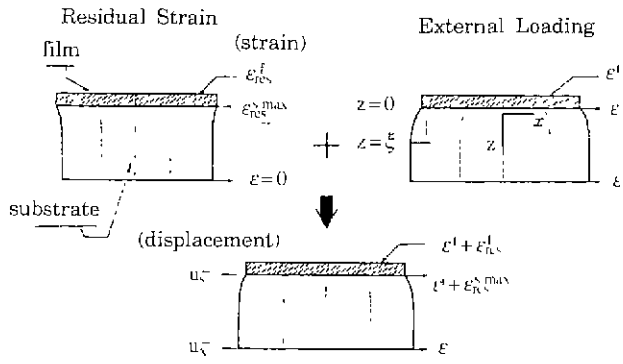

Fig. 2. Effects of film residual stress and film constraint on x-directional strain state in substrate.

straining, and so we take its effect into account by adding the film residual strain ε_{res}^{f} linearly to the strains, ε' and $-\nu_s\varepsilon$, as seen in Fig. 2:

$$\varepsilon_x^f = \varepsilon_{res}^f + \varepsilon', \qquad \varepsilon_y^f = \varepsilon_{res}^f - \nu_s\varepsilon \ . \tag{11}$$

At this point, to restore the force equilibrium state disturbed by the film residual stress, the stress of an opposite sign develops in the near-interface region of the substrate. If the substrate residual stress is assumed to decrease linearly from the interface to z=ξ, it can be expressed in terms of the film residual stress through the force equilibrium condition, $F_f + F_s = 0$. In consequence, the maximum substrate residual strain, $\varepsilon_{res}^{s,max}$, believed to develop at the interface, is determined with sign opposite to the film residual strain as follows:

$$\varepsilon_{res}^{s,max} = -2\frac{t}{\xi}\frac{(1-\nu_s)}{(1-\nu_f)}\frac{E_f}{E_s}\varepsilon_{res}^{f} \ . \tag{12}$$

Though no external load is applied, the substrate strain at the near-interface has some contributions from the residual stress as mentioned above. The first-order differential terms in Eq. (10), i.e., substrate strains, are thus determined as indicated in Fig. 2 by adding linearly the contributions of the residual stress ($\varepsilon_{res}^{s,max}$) and of the external tensile load (ε and ε'):

$$\frac{du_s^+}{dx} = \varepsilon_{res}^{s,max} + \varepsilon', \qquad \frac{du_s^-}{dx} = \varepsilon \ . \tag{13}$$

We can derive ε' in terms of σ_x^f and ε by using condition (11). Then, by applying condition (13) to Eq. (10), the governing equation of film tensile stress is obtained as

$$\frac{d^2\sigma_x^f(x)}{dx^2} = \frac{2G_s}{\xi t}\left(\frac{1-\nu_f^2}{E_f}\sigma_x^f(x) - (1+\nu_f)\varepsilon_{res}^{f} + \varepsilon_{res}^{s,max} - (1-\nu_s\nu_f)\varepsilon\right). \tag{14}$$

Consider the case in which two cracks a distance λ apart have formed in the film. In this geometry, the film tensile stress is zero at both film edges ($x=\pm\lambda/2$) and the shear stress has an antisymmetric distribution along x direction. By applying these boundary conditions, the solution of Eq. (14) is determined in terms of crack spacing λ and external strain ε as follows:

$$\sigma_x^f(x) = F(\varepsilon_{res}^{f},\ \varepsilon)\left(1 - \frac{\cosh\alpha x}{\cosh(\alpha\lambda/2)}\right) \ . \tag{15}$$

Through the relation (7),

$$\tau_i(x) = F(\varepsilon_{res}^{f},\ \varepsilon)\,\alpha t\frac{\sinh\alpha x}{\cosh(\alpha\lambda/2)} \tag{16}$$

where

$$F(\varepsilon_{res}^{f},\ \varepsilon) = \frac{E_f}{(1-\nu_f)}\varepsilon_{res}^{f} + \frac{2t}{\xi}\frac{(1-\nu_s)}{(1-\nu_f)^2(1+\nu_f)}\frac{E_f^2}{E_s}\varepsilon_{res}^{f} + \frac{1-\nu_s\nu_f}{1-\nu_f^2}E_f\varepsilon \quad \text{and}$$

$$\alpha = \sqrt{\frac{G_s}{E_f}\frac{2}{\xi t}(1-\nu_f^2)} \ .$$

In the early stage of straining, because the rate of increase of the tensile stress with straining is higher than that of the interface shear stress, the tensile stress easily reaches the critical fracture strength of the film so that film cracking occurs. Then, for the further film cracking to continue, additional tensile stress must be transferred to film to overcome the stress relief resulting from film cracking. This additional stress transfer is accomplished by the increase of interface shear stress with straining. But, as the crack spacing decreases, the rate of increase of film tensile stress becomes significantly lower than that of interface shear stress. Thus film separation occurs before film cracking if the interface shear stress reaches the critical shear strength τ_d before the film tensile stress reaches σ_c. Then, additional stress transfer becomes impossible because of interface damage, and so film cracking stops and reaches the saturation state. The maximum value of interface shear stress deveolped at the stoppage of film cracking can be estimated as the interface shear strength τ_d through the following equation if the saturated values of strain and crack spacing, ε_s and λ_s, are experimentally measured.

$$\tau_d = \tau_i(x = \frac{\lambda_s}{2}) = F(\varepsilon_{res}^{f},\ \varepsilon_s)\,\alpha t\cdot\tanh\frac{\alpha\lambda_s}{2} \tag{17}$$

III. Experiments

The validity of the analyses presented above was tested on DLC films deposited on WC-Co K20 and annealed 1050 Al substrates. Ar-plasma pre-etching time was varied in order to investigate the effect of pre-etching time on interface adhesion. WC-Co substrates (12 mm length × 12 mm width × 3 mm thickness) and dogbone-shaped Al substrates (25 mm × 7 mm × 3 mm) were mechanically polished, and then ultrasonically cleaned sequentially in trichloroethylene, acetone, methanol and ethanol. The DLC films were deposited by plasma-enhanced CVD (PECVD). Before depositing DLC films on WC-Co substrates, the chamber was evacuated to a pressure of 7.0×10^{-4} torr and then backfilled with Ar gas to a pressure of 0.15 torr by flowing Ar gas at 14 sccm, followed by plasma pre-etching of the substrate. Then the composition of gas was changed in a few seconds from Ar 14 sccm and CH_4 0 sccm to Ar 0 sccm and CH_4 14 sccm. After this procedure, DLC films were deposited under an initial pressure of CH_4 0.3 torr.

And we deposited the DLC films on Al substrates under a CH_4 plasma atmosphere of 0.28 torr for 45 minutes, proceded by the pre-etching: 0, 5, 15, 30 and 60 minutes under an Ar plasma atmosphere of 0.17 torr. To evaluate the residual stress in the film, we deposited the DLC film on the {001} flat silicon wafer of thickness 200 μm and aspect ratio at least 13. After the deposition, the curvature of substrate was measured by laser deflection method and then the residual stress in the film was es-

timated.[19] The film thickness was measured using an α-step profilometer.

All the critical load measurements were performed by the scratch tester equipped with an acoustic emission (AE) detector. The detailed experimental conditions are as follows. We deposited the DLC films for 15, 30 and 45 minutes with a plasma etching time of 15 minutes. Scratch tests were performed on each specimen. The Rockwell C diamond indenter (conical angle: 120°; hemispherical tip of 200 μm radius) of the test apparatus was drawn over the sample surface with continuously increasing normal load. The loading rate was 100 N/min and the scratching speed was 10 mm/min. The indenting load, tangential friction force, friction coefficient and AE signal from the diamond tip were continually monitored. We then deposited the DLC films for 30 minutes with plasma etching times of 5, 15 and 30 minutes. Scratch tests were carried out with scratching speeds 5, 10, 15 and 20 mm/min, under constant loading rate 100 N/min and indenter tip radius 200 μm.

To obtain the relation of crack spacing to strain, the prepared specimens were pulled with a tensile tester. The substrate was removed from the straining stage and examined with an optical microscope in order to measure film crack spacing. This process was repeated to obtain data for the wide range of strain: the strains were measured each time by attaching an extensometer to the substrate, and the crack spacing was obtained as an average value of three different data points. The film cracking behavior with external strain is shown in Fig. 3. The newly developed cracks can have smaller width than existing cracks; as the crack patterns saturate, the crack widths increase and become comparable. This is because its increase accommodates most of the substrate deformation and the film does not deform any more after this point.

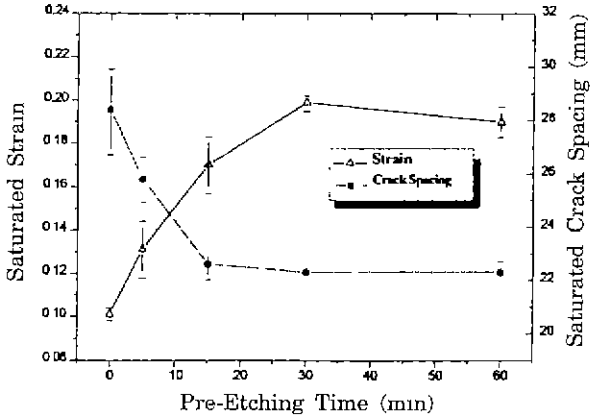

Fig. 3. Dependency of saturated strain and crack spacing on Ar plasma pre-etching time.

IV. Results and Discussion

1. Scratch test

In differently deposited specimens, the detailed experimental results are shown in Table 1. As listed in Table 2, the critical loads decrease significantly with the increase of film thickness. In general, if we assume that the adhesion is the same and the critical load is determined by the extent of deformation, an increased film thickness requires an increased indenting load to obtain the same deformation, so that the critical load increases with the film thickness.[20,21] But, considering the residual stress effect in the film, the variation of critical load with film thickness may be described in another way. In our experiment (see Table 1), the estimated compressive residual stresses are 813, 669 and 632 MPa for film thicknesses of 0 78, 1.31 and 2.32 μm, respectively. These residual stresses decrease as film thickness increases, but the elastic deformation energies stored in the film ($\propto \sigma_{res}^2 \cdot t$) due to only the residual stress increase. Thus the critical loads decrease with increasing film thickness.

Table 2 illustrates the experimental results of differently pre-etched specimens. Film thicknesses were 1.16, 1.31 and 1.30 μm with the increase of etching time, and the measured film compressive residual stresses were 741, 733 and 735 MPa, respectively. As listed in Table 2, the critical loads decrease distinctly with increasing scratching speed and increase with increasing etching time. The latter effect is mainly due to better cleanness of the surface as the etching time increases. The former effect is probably because, when scratching speed increases under constant loading rate, the probability of encountering defects in the film within a certain load range increases, so that critical load decreases. With scratching speeds above 15 mm/min, however, critical load apparently did not decrease with increasing scratching speed. It is likely that the film may wear at

Table 1. Experimental Results Obtained at Indenter tip Radius 200 μm and Theoretically Evaluated work of Adhesion (W) for DLC Films Deposited on WC-Co Substrates (loading rate: 100 N/min, scratching speed: 10 mm/min)

Deposition time min	Film thickness μm	Residual stress MPa	Critical load N	Friction coeff.	Contact radius μm	Work of adhesion J/m^2
15	0.78	-813	33.32	0.0797	25.6	17.87
30	1.31	-669	30.70	0.0552	24.6	17.81
45	2.32	-632	12.50	0.0425	15.7	17.90

Table 2. Experimental Results Obtained at Plasma Etching time 5, 15 and 30 minutes and Theoretically Evaluated work of Adhesion (W) for DLC Films Deposited on WC-Co Substrates (indenter tip radius: 200 μm, loading rate: 100 N/min)

Plasma etching time min	Scratching speed mm/min	Film thickness μm	Critical load N	Friction coeff.	Contact radius μm	Work of adhesion J/m^2
5	5	1.16	37.21	0.0622	27.0	19.50
	10		22.08	0.0593	20.8	17.60
	15		13.63	0.0693	16.4	19.21
	20		13.77	0.0591	16.5	16.08
15	5	1.31	38.67	0.0606	27.6	20.07
	10		30.70	0.0552	24.6	17.78
	15		12.13	0.0493	15.4	12.85
	20		11.81	0.0513	15.2	13.39
30	5	1.30	66.83	0.0825	36.2	27.16
	10		51.86	0.0832	31.9	27.17
	15		33.89	0 0787	25.8	24.88
	20		28.01	0.0715	23.5	21.91

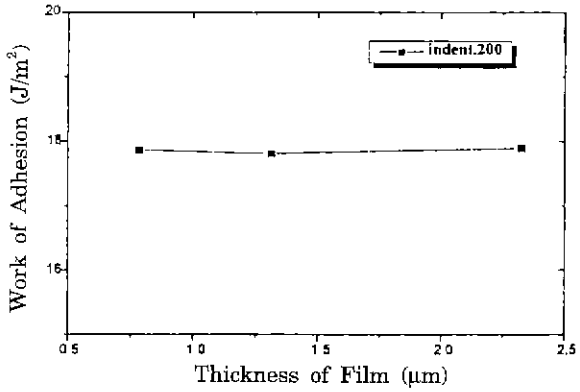

Fig. 4. Variation of work of adhesion with film thickness for indenter tip radius 200 μm.

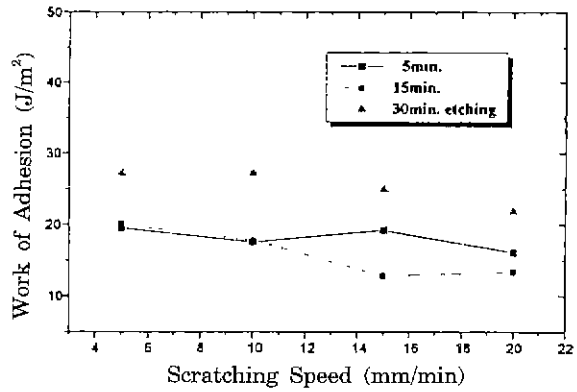

Fig. 5. Variations of work of adhesion with scratching speed for plasma etching time 5, 15 and 30 minutes.

higher scratching speeds. In general when wear occurs between materials in contact, the softer material is deformed by debris on contact surface, or the asperities of the surface are deformed. Indenting load is consumed in these deformations. So the measured critical load will be greater than that expected.

By taking Poisson's ratio and Young's modulus for the film as 0.25 and 200 GPa, respectively, we estimated the change in elastic deformation energy in a unit volume of film with the change of film thickness. By linear regression of data, we obtained the value of γ_f/c calculated from Eq. (6): 8.79 J/m^3 with indenter tip radius 200 μm. Using this value, we evaluated the work of adhesion in differently deposited specimens (see Table 1). The evaluated work of adhesions using tip radius 200 μm were 17.87, 17.81 and 17.90 J/m^2, nearly constant regardless of the change in film thickness as shown in Fig. 4.

Using the value of γ_f/c obtained with tip radius 200 μm, we evaluated the work of adhesion for different plasma etching times, as listed in Table 2 and shown in Fig. 5. The work of adhesion increases: 18.6, 18.9 and 27.2 J/m^2 with plasma etching times of 5, 15 and 30 minutes, respectively. The work of adhesion was evaluated constantly except at scratching speeds 15 and 20 mm/min. This discrepancy may result from the wear described above. Therefore, when considering the scratching speed range in which the wear is not severe, we could evaluate the quite constant work of adhesion not influenced by any effect of scratching speed. Furthermore, the constant work of adhesion could be assessed eliminating the film thickness effect in the current stress analysis by extracting the surface energy generated by film spallation. These experimental results mean that interface adhesion strength can be analytically evaluated as work of adhesion from the critical load, which is dependent on various parameters besides adhesion. This evaluation gives

us reliable data on interface adhesion strength that exclude the effects of external experimental factors.

2. *Film cracking test*

ε_s-λ_s data estimated from the experimentally obtained ε-λ data for each etching time are plotted in Fig. 3. The test results show that the saturated strain, ε_s, increases from 0.1 to 0.2 with increasing pre-etching time, but the saturated crack spacing, λ_s, decreases from 29 μm to 22 μm as listed in Table 3. We take the elastic modulus of Al substrate as 70 GPa and its Poisson's ratio as 0.35, respectively.[22]

The measurement of film fracture strain ε^*, which is determined by observing whether or not the film has cracked after several small strains, shows that ε^* is 0.012 for DLC films deposited for 45 minutes (the film cracks formed in the range $\varepsilon > 0.012$), and the fracture strength σ_c is then estimated as 1.8 GPa ($\sigma_c = E_f\varepsilon^*$), as in other literature.[23] However, initial cracking occurs at a strain less than 0.011 for the 60 minute-deposited film. This tendency for film fracture strength to decrease with increasing film thickness has been attributed to the higher probability of the existence of larger defects in the thicker film.[24] However, in amorphous film such as DLC film, the tendency is probably also affected to some extent by compressive residual stress in the film, which decreases with increasing film thickness. In other words, the decrease of compressive residual stress in the film makes film fracture easier. This argument is confirmed by the film residual stress data in Table 1 which show that the residual stress decreases with increasing film thickness. Substrate residual stress estimated through Eq. (12) was considered negligible compared to the other terms in Eq. (14).

To determine ξ, we fit the experimental crack spacing vs. strain data to the following relation, which was derived on the assumption that film cracking occurs in the middle of the film, x=0, where maximum film tensile stress develops, when the maximum tensile stress in a film having two cracks a distance λ apart is equal to the film fracture strength σ_c. The film fracture strength σ_c is determined not by the simple Hooke's law ($\sigma_c = E_f\varepsilon^*$) but by Eq. (15) under the initial film cracking conditions, i.e., crack spacing is infinite and strain is ε^*

$$\lambda = \frac{2}{\alpha}\cosh^{-1}\frac{\frac{1+\nu_f}{1-\nu_s\nu_f}\varepsilon_{res}^f + \varepsilon}{\varepsilon - \varepsilon^*} \tag{18}$$

By fitting ε vs. λ data to relation (18), we obtained ξ=120 μm and α=0.0369 μm^{-1} for the DLC film of 2 μm thickness. The film-affected depth in the substrate and α decreases as film thickness increases.

Interface shear strength was evaluated quantitatively through Eq. (17) using the ε_s-λ_s data as shown in Fig. 6. The results show that the strength increases with pre-etching time but its rate of increase becomes lower in the 15-minute pre-etching and finally reaches an almost constant value after the 30-minute pre-etching. The interface shear strength of DLC films on Al without pre-etching is estimated as 480 MPa, and the values increase up to 760 MPa with a 30-minute pre-etching, which means an increase of adhesion strength by a factor of 1.6. However, the magnitude of interface shear strength depends on the measured parameters ε^* and E_f, and so it is noted that a reliable value of E_f must be presented to ensure the precision of the interface shear strength. The improvement of interface shear strength with increasing pre-etching time is thought to be due to the removal of surface impurity layers such as oxides etc., and may also be related to increasing plasma temperature. These results, as shown in Fig. 6, are in good agreement with the general prediction that interface adhesion is improved by etching the substrate surface. As Fig. 6 shows, 30-minute pre-etching is sufficient for the present DLC/Al system.

From the experimental fact that ε_s and λ_s have a clear dependency on adhesion, i.e., ε_s increases and λ_s decreases with pre-etching time, we know that though our final goal is the interface shear strength, ε_s and λ_s can be taken into consideration as standard parameters for the qualitative comparison of adhesion. However, as plotted in Fig. 7, ε_s and λ_s are interrelated by the following modified form of Eq. (18).

Table 3. Film deposition conditions and measured properties for 45 minute-deposited DLC films

Etching time min	Plasma temp. °C	Residual stress MPa	Film thickness μm
0	70	-644	2.04
5	80	-750	2.03
15	100	-716	2.17
30	100	-624	2.01
60	110	-665	1.97

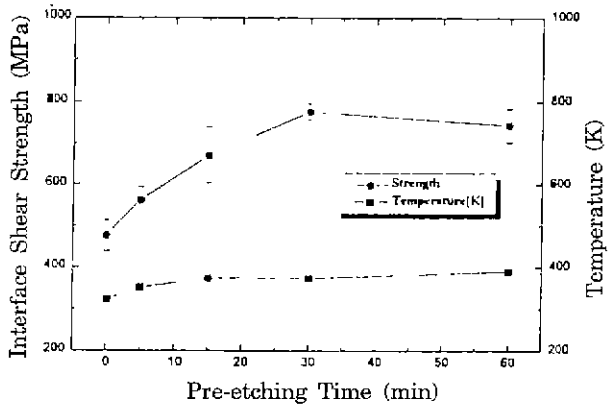

Fig. 6. Variations of interface shear strength and plasma temperature with pre-etching time.

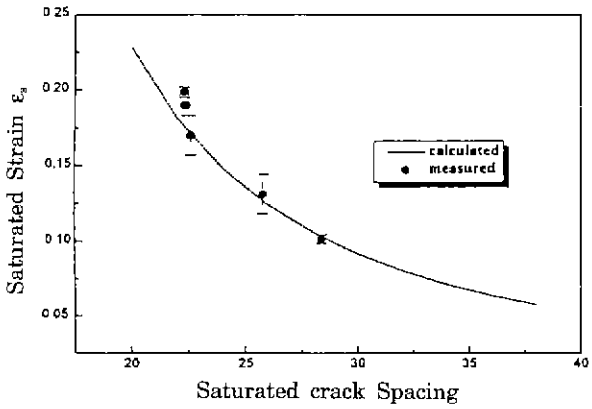

Fig. 7. Correlation between saturated strain, ε_s, and crack spacing, λ_s : ε_s is inversely proportional to λ_s.

$$\varepsilon_s = \frac{A + \varepsilon^* \cosh(\alpha\lambda_s/2)}{\cosh(\alpha\lambda_s/2) - 1} \tag{19}$$

ε_s is closely related to λ_s with an inverse-proportional relationship. As seen in Fig. 7, since one parameter can be found from knowledge of the other through Eq. (19), a single parameter is sufficient to describe the interface adhesion qualitatively. Using ε_s will be more effective than λ_s, because ε_s is more sensitive to interface adhesion than λ_s is.

V. Conclusions

1) In a scratch test, the stress state in the material ahead of the spherical indenter can be described by considering the blister stress caused by the plastic deformation of the material and the friction stress.

2) Through stress analysis, the strain of the film can be described by using the strain-matching criterion and the constant strain over the film thickness. In addition, by using the strain in the film, we could evaluate the work of adhesion through the Griffith energy-balance approach:

$$W = \frac{E_f}{2}\left(\sum \varepsilon^2\right) t - \frac{2(\pi+2)}{\pi}\frac{\gamma_f}{c} t \ .$$

3) The constant work of adhesion with increasing etching time was evaluated irrespective of various scratching speeds. These results clearly show the increase of adhesion with increasing plasma etching time. In addition, the evaluated work of adhesions with varying film thickness were about 17.86 J/m^2 irrespective of film thickness.

4) In film cracking test, by applying shear lag theory to the interface of hard film deposited on ductile metal substrate, the distributions of the interface shear stress and the film tensile stress can be expressed in terms of the external strain ε and the crack spacing λ.

5) Film cracks devolp no further after some straining because interface failure occurs preferentially to film cracking by the excessive interface shear stress applied to the interface. By using the distribution of interface shear stress analyzed above, interface adhesion strength can be evaluated from the parameters ε_s and λ_s in terms of interface shear strength:

$$\tau_d = F(\varepsilon_{fes}^f, \varepsilon_s)\alpha t \cdot \tanh\frac{\alpha\lambda_s}{2} \ .$$

6) According to the current stress analysis, for DLC/Al, interface shear strength is estimated to increase from 480 MPa for no etching up to 760 MPa for 30-minute etching, after which it becomes constant, This result shows that 30-minute pre-etching is sufficient for a given DLC/Al system.

References

1. D. C. Agrawal and R. Raj, "Measurement of the Ultimate Shear Strength of a Metal-Ceramic Interface," *Acta Metall.*, **37**[4], 1265 (1989).
2. B. -Y. Ting, W. O. Winer and S. Ramalingam, "A Semi-Quantitative Method for Thin Film Adhesion Measurement," *J. Trib.*, **107**, 472 (1985).
3. T. S. Chow, C. A. Liu and R. C. Penwell, "Direct Determination of Interfacial Energy between Brittle and Polymeric Films," *J. Polym. Sci. Polym. Phys.*, **14**, 1305 (1976).
4. L. Chandra and T. W. Clyne, "Characterization of the Strength and Adhesion of Diamond Films on Metallic Substrates Using a Substrate Plastic Technique," *Diam. Relat. Mater.*, **3**, 791 (1994).
5. M. D. Bentzon, C. Barholm-Hansen and J. Bindslev Hansen, "Interfacial Shear Strength of Diamond-like Carbon Coatings Deposited on Metals," *Diam. Relat. Mater.*, **4**, 787 (1995).
6. K. Zeng, K. Breder and D. J. Rowliffe, "The Herzian Stress Field and Formation of Cone Cracks 1. Theoretical Approach," *Acta Metall. Mater.*, **40**[10], 2595 (1992).
7. G. M. Hamilton and L. E. Goodman, "The Stress Field Created by a Circular Sliding Contact," *J. Appl. Mech.*, **33**, 371 (1966).
8. J. Boussinesq. "Applications des Potentials," *Mem. Soc. Sci. Agric.*, **13**, 99 (1885).
9. S. Way and E. Pittsburgh, "Some Observations on the Theory of Contact Pressures," *J. Appl. Mech.*, **7**, 147 (1940).
10. E. H. Yoffe, "Elastic Stress Fields Caused by Indenting Brittle Materials," *Phil. Mag. A*, **46**[4], 617 (1982).
11. A. K. Ghosal and S. K. Biswas, "Examination of Stress Fields in Elastic-Plastic Indentations," *Phil. Mag. A*, **67**[3], 371 (1993).
12. H. -S. Park and D. Kwon, "Micromechanical Analysis of Scratch Test for Evaluation of Adhesion Strength for Hard Thin Films," *J. Kor. Inst. Met. Mater.*, **34**[11], 1415 (1996).
13. M. S. Hu, M. D. Thouless and A. G. Evans, "The Decohesion of Thin Films from Brittle Substrates," *Acta Metall.*, **36**[5], 1301 (1988).
14. M. A. Voronkin, S. N. Dub, I. N. Lupich and B. A.

Maslyuk, "Determination of Adhesion Strength between a Carbon Film and a Polymeric Substrate," *Diam. Relat. Mater.*, **3**, 116 (1993).
15. M. S. Hu and A. G. Evans, "The Cracking and Decohesion of Thin Films on Ductile Substrates," *Acta Metall.*, **37**[3], 917 (1989).
16. H. L. Cox, "The Elasticity and Strength of Paper and Other Fibrous Materials," *Br. J. Appl. Phy.*, **3**, 72 (1952).
17. J. -h. Jeong and D. Kwon, "Interfacial Adhesion Assessment for Thin Films through the Stress Analysis of Tensile Plastic Straining Method," *J. Kor. Inst. Met. Mater.*, **34**[10], 1290 (1996).
18. F Erdogan and M B. Civelek, "Contact Problem for an Elastic Reinforcement Bonded to an Elastic Plate," *J. Appl. Mech.*, **42**, 1014 (1974).
19. G. G. Stoney, "The Tension of Metallic Films Deposited by Electrolysis," *Proc. R. Soc. London A*, **82**, 172 (1909).
20. P. A. Steinmann, Y. Tardy and H. E. Hintermann, "Adhesion Testing by the Scratch Test: the Influence of Intrinsic and Extrinsic Parameters on the Critical Load," *Thin Solid Films*, **154**, 333 (1987).
21. J. Valli, "A Review of Adhesion Test Methods for Thin Hard Coatngs," *J. Vac Sci. Technol. A*, **4**, 3007 (1986).
22. E. A. Brandes, *Smithells Metals Reference Book*, 6th Ed., Butterworth & Co., 15-2 (1983).
23 P. D. Garrett and B. K. Daniels, "Tensile Stress-Strain Properties of a-C.H (Diamond-like Carbon) Thin Films," *MRS Symp. Proc.*, Materials Research Society, Pittsburgh, PA, **239**, 659-664 (1992).
24. P. H. Wojciechowski and M. S. Mendolia, "On the Multiple Fracture of Low-elongation Thin Films Deposited on High-elongation Substrate," *J. Vac. Sci. Technol. A*, **7**[3], 1282 (1989).